Journal of Engineering Physics and Thermophysics, Vol. 70, No. 2, 1997

MODELING OF TEMPERATURE FIELD OF "BESSER" CONCRETE BLOCKS UNDER STANDARD FIRE CONDITIONS

V. I. Nikolaev

UDC 536.24

The unsteady temperature field in a structural element of a load-bearing building wall constructed of vibropressed concrete blocks is investigated. Different variants of thermal loading under standard fire conditions are considered. Calculations made are based on the problem-oriented FEM-package NIKABT.

INTRODUCTION

The present work is devoted to investigation of the heat-insulating capacity of a multilayer wall built of vibropressed hollow blocks (the technology of the firm "Besser"). Investigations were made by order of the joint venture "Besser–Belarus." The goal was to calculate the temperature field in the wall cross-section under standard fire conditions for normalized time. Calculations were based on the finite-element method (FEM) realized in the form of the problem-oriented software package NIKABT. In general, the package was created for modeling of convection and diffusion processes in channels and structural elements of complex geometry [1, 2]. The physical model of the heat-conduction process in the structure under consideration was based on a model of unsteady heat conduction with allowance for changing thermophysical properties of the structural materials: thermal conductivity, heat capacity, and densities of air, concrete, and mineral-wool curing mats. The main requirements and norms adopted in civil engineering and used in the present investigation are reported in [3-9].

1. MATHEMATICAL MODEL AND NUMERICAL METHOD OF SOLUTION

The space-time distribution of temperature can be represented, with use of traditional designations and tensor symbols, as

$$\rho c_p \frac{\partial \overline{T}}{\partial t} = \frac{\partial}{\partial x_i}\left(\lambda \frac{\partial \overline{T}}{\partial x_i}\right) + \overline{F}_q , \tag{1.1}$$

where λ is thermal conductivity, $\overline{F}_q$ is a heat source or heat sink, depending on the physical process under consideration.

Equation (1.1) describes various thermal diffusion processes within the framework of the adopted assumptions and concepts. Differences in solutions are attributable only to initial and boundary conditions, whose correct specification determines the stability, accuracy, and convergence of the solution obtained. It is known that a test of the legitimacy of a formulated boundary-value problem is, in the general case, the proof of a uniqueness and existence theorem. However, in practice this proof is hard to realize and most often it is easier to obtain a solution through numerical simulation and to verify it by comparing with experiment.

The modeled region represented a three-layer wall made of vibropressed blocks, whose calculated structural element is shown in Figs. 1 and 2. At the left and right boundaries of the integration region the symmetry conditions were prescribed. As boundary and initial conditions, we adopted third-kind thermal conditions (convective heat

Institute of Radioenvironmental Problems, Academy of Sciences of Belarus, Minsk. Translated from Inzhenerno-Fizicheskii Zhurnal, Vol. 70, No. 2, pp. 330-339, March-April, 1997. Original article submitted July 4, 1995.

 1062-0125/97/7002-0332$18.00

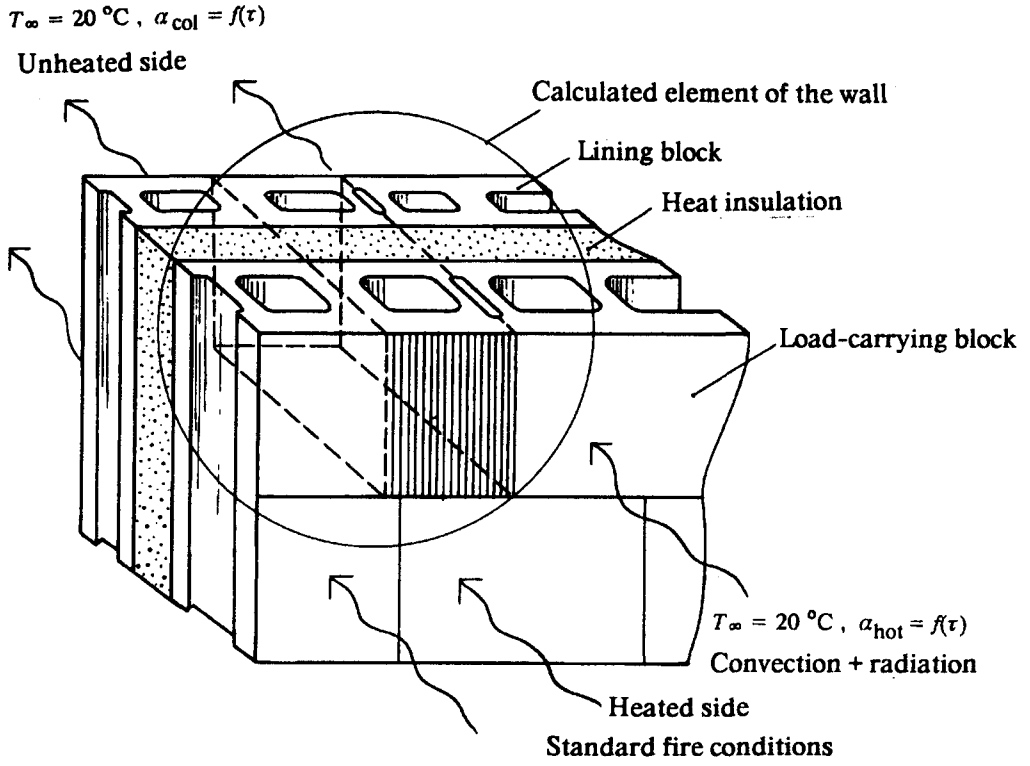

Fig. 1. Structural element and heat transfer scheme for calculation of fire resistance of the three-layer wall made of "BESSER" concrete blocks.

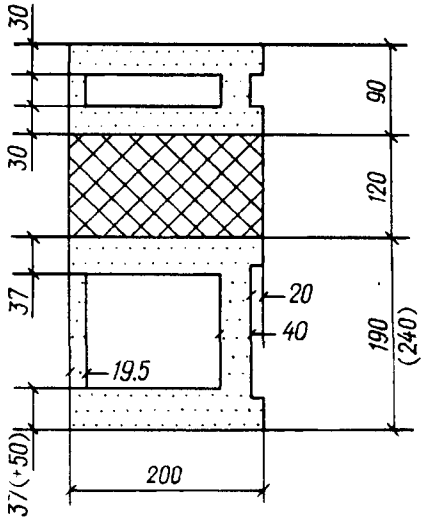

Fig. 2. Calculation scheme for the three-layer wall (the dimensions in parentheses are for the second variant).

transfer) with heated and cooled sides of the wall (the lower and upper boundaries of the integration cell in Fig. 1) with allowance for radiative heat transfer as viewed from a fire.

Method of Solution. Numerical integration was conducted using the finite-element method (FEM), which, as known, is based on seeking the extremum of a functional corresponding to the initial differential equation. It was first published by M. J. Terner, R. Kluzh, G. Martin, L. J. Topp, and later was advanced by O. Zenkevich, L. Ciegerlind, G. Streng, D. Norry, and others.

The main idea of the FEM lies in representing any continuous, in some region, quantity by a discrete model (DM), which is built using a finite set of piecewise continuous functions determined for a finite number of subregions. To construct the DM, a region is subdivided into a finite number of elements which, in totality,

approximate its form. Next, with the aid of nodal values a polynomial is built which determines the desired quantity inside an element. The value at each nodal point is considered to be variable and must be determined.

System of Nodal Equations. In order to obtain a discrete analog of a continuum, in which thermal diffusion processes are determined by basic equation (1.1), we write the generalized diffusion equation parabolized with respect to the Z-coordinate, which in our case has the physical meaning of time, in the following form:

$$G_1 \frac{\partial \Phi}{\partial z} = \frac{\partial}{\partial x}\left(G_2 \frac{\partial \Phi}{\partial x}\right) + \frac{\partial}{\partial y}\left(G_2 \frac{\partial \Phi}{\partial y}\right) + Q. \tag{1.2}$$

Using the Galerkin method and applying the approximation

$$\Phi(x, y) = \sum_{i=1}^{m} N_i(x, y)\, \Phi_i(z), \tag{1.3}$$

where m is the number of nodes in the element, we can write the Galerkin formula as follows:

$$\iint_{\Omega} N_i \left[\frac{\partial}{\partial x}\left(G_2 \frac{\partial \Phi}{\partial x}\right) + \frac{\partial}{\partial y}\left(G_2 \frac{\partial \Phi}{\partial y}\right) + Q - G_1 \frac{\partial \Phi}{\partial z}\right] d\Omega = 0. \tag{1.4}$$

Applying Green's transformations for each of the terms in this formula, we arrive at

$$\iint_{\Omega} N_i \left[\frac{\partial}{\partial x}\left(G_2 \frac{\partial \Phi}{\partial x}\right)\right] dxdz = \iint_{\Gamma} \left[N_i G_2 \frac{\partial \Phi}{\partial x}\right] \int_{A}^{B} dz - \iint_{\Omega} \left[\frac{\partial N_i}{\partial x} G_2 \frac{\partial \Phi}{\partial x}\right] dxdz =$$

$$\int_{\Gamma} \left[N_i G_2 \frac{\partial \Phi}{\partial x}\right] n_x d\Gamma - \iint_{\Omega} \left[G_2 \frac{\partial N_i}{\partial x} \frac{\partial \Phi}{\partial x}\right] dxdz. \tag{1.5}$$

Adopting a similar procedure for the second term in formula (1.4), we obtain the following expression

$$\iint_{\Omega} \left[G_2 \frac{\partial N_i}{\partial x} \frac{\partial \Phi}{\partial x} + \frac{\partial N_i}{\partial y} \frac{\partial \Phi}{\partial y}\right] d\Omega - \iint_{\Omega} N_i Q d\Omega +$$

$$+ \iint_{\Omega} N_i G_1 \frac{\partial \Phi}{\partial z} d\Omega - \int_{\Gamma} N_i q_{\Gamma} \frac{\partial \Phi}{\partial x} d\Gamma = 0. \tag{1.6}$$

Integration is performed over the domain of elements, since in the remaining part of the domain $N_i = 0$. Substituting the expression for $\Phi(x, y)$, using the generally accepted notation, and writing in matrix form, we obtain

$$[C] \frac{d\{\Phi\}}{dz} + [K]\{\Phi\} + \{F\} = 0. \tag{1.7}$$

The contribution of each element to matrices $[K]$, $[C]$, and $\{F\}$ is expressed by the following formulas:

$$[C]^{(e)} = \int_{\Omega} G_1 [N]^T [N] d\Omega; \tag{1.8}$$

$$[K]^{(e)} = \int_{\Omega} [B]^T [D] [B] d\Omega + \int_{S_2} \kappa [N]^T [N] dS; \tag{1.9}$$

$$\{F\}^{(e)} = -\int_{\Omega} Q [N]^T d\Omega + \int_{S_1} q_1 [N]^T dS - \int_{S_2} \kappa \Phi_{\infty} [N]^T dS,$$

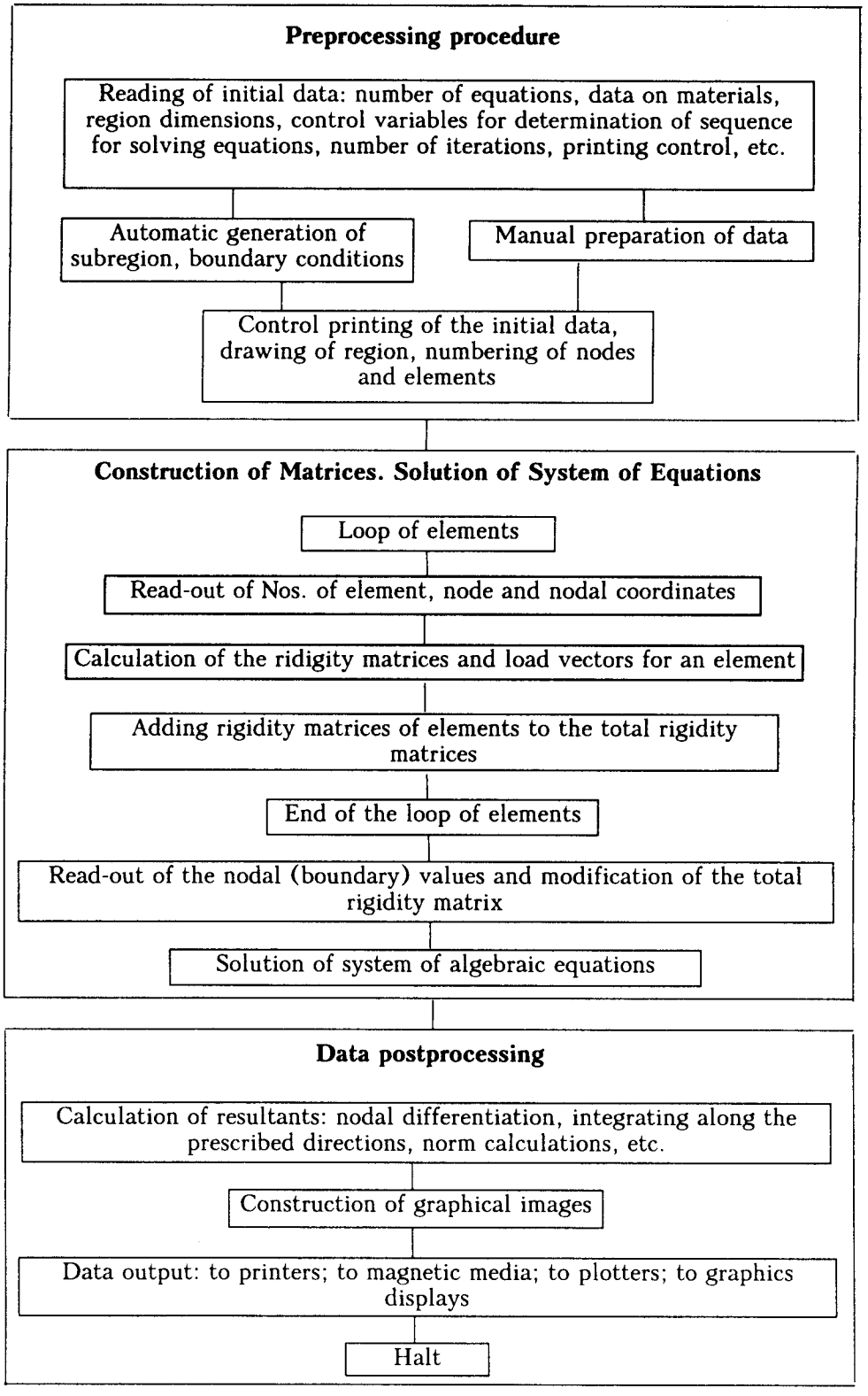

Fig. 3. Block-diagram of the FEM software implementation.

where S_1 and S_2 are the surfaces on which the second- and third-kind conditions are given, respectively.

The boundary conditions with zero heat flux are taken into account, in the usual way, in integral equations at all boundary nodes where heat flux is absent.

The overall rigidity matrix $[K]$ is obtained by performing simple summation over all elements. Similarly, the damping matrix $[C]$ and the global load vector $\{F\}$ are formed. The matrix $[N]^T$ is the transposed matrix $[N]$, while $[B]$ and $[B]^T$ are the direct and transposed matrices of the gradients, $[D]$ is the conductivity matrix, which in the general case of an anisotropic medium is:

$$[D] = \begin{bmatrix} \lambda_{xx} & 0 & 0 \\ 0 & \lambda_{yy} & 0 \\ 0 & 0 & \lambda_{zz} \end{bmatrix}. \tag{1.10}$$

Integration of the initial equations downstream was performed in accordance with a purely implicit two-layer scheme

$$K_{i+1}\,\Phi_{i+1} + C_{i+1}\,(\Phi_{i+1} - \Phi_i)/\Delta z - F_{i+1} = 0\,. \tag{1.11}$$

The system is linear relative to Φ_i and is solved by iteration according to the scheme

$$\begin{aligned} &K_{i+1}^s\,\Phi_{i+1}^{s+1} + C_{i+1}^s\,(\Phi_{i+1}^{s+1} - \Phi_i^s)/\Delta z - F_{i+1}^s = 0\,; \\ &\left[K_{i+1}^s + C_{i+1}^s/\Delta z\right]\Phi_{i+1}^{s+1} = C_{i+1}^s\,\Phi_i^s/\Delta z + F_{i+1}^s\,. \end{aligned} \tag{1.12}$$

Program Structure. The structure of a general program or software package implementing the FEM includes the following basic stages: reading of the initial data; generation of a discrete finite-element model; construction of an overall rigidity matrix; solution of a system of algebraic equations; postprocessing of digital data; and output of results. The above stages are represented by the general block diagram in Fig. 3.

In the general program, the basic stages of implementation were subprograms. The latter provided for calculation of the form functions, integration by quadrature formulas, determination of the width of the matrix band, calculation of coefficients and source terms with the aid of basis functions, etc. As the program structure is modular, it allows rather quick reconstruction of the available program by changing this or that functioning block. This refers to the modula for calculation of the form functions or solution of a system of algebraic equations and to the digital data pre- and postprocessing modules. In the course of developing the program we used different methods in constructing a discrete model, solving a system of algebraic equations, and data postprocessing, data output to peripherals (monitor screen, printer, or plotter).

The concrete physical form of a differential equation (expressions for coefficients and source terms) is determined by the module for coefficient calculation and construction of the overall rigidity matrix and the load vector.

Software Implementation. Realization of the FEM method is involves with construction of a discrete analog of a continuum with the aid of a finite-element network. The efficiency of calculations depends, in many respects, on the quality of region subdivision into elements. In principle, the order of node numbering is of no importance, but real computer capacities impose restrictions on the band width of the matrix of the system of linear algebraic equations (SLAE), and, therefore, there is a need to optimize the procedure of node numbering.

Different methods exist for optimal subdivision of a region, and one of the most effective and widely used methods is that of numbering the nodes of a discrete region from left to right and downward in a zigzag manner. This results in the smallest band width of the matrix for a given number of elements along the vertical. Using this procedure as a basis for algorithmic representation of the process of node numbering, we obtain a minimal band width of the matrix. In the case of a composite region, each subregion is subdivided, using the above procedure, and the band width of the overall matrix of coefficients is subjected to straight-through optimization.

The main specific feature of the FEM is a large volume of arithmetic operations, which imposes definite requirements on computer internal storage and efficiency. Despite concrete methods and approaches to software implementation, the block diagram of the FEM program possesses some general features. The number of integration points depends on the polynomial order and is introduced together with the node information. The order of an element is determined when prescribing its geometry and performing interpolation of the desired quantity by its nodal values. Nodal coordinates can be determined either manually or by an automatic spectrum generator.

Gaussian coordinates of integration points and weight coefficients are calculated, as a rule, using a special program.

Construction of Jacobi matrices and their reciprocals as well as their determinants is carried out in the cycle of calculating the coefficients of the matrices of elements. The values of the form functions and their derivatives required for this are determined in a special subprogram, in which a function is chosen from a corresponding set with the aid of conventional transition operators.

Calculation of the partial derivatives by global coordinates is carried out in a separate subprogram, where the column-vector of the derivatives $\partial N_i/\partial\xi$ and $\partial N_i/\partial\eta$ is multiplied by a Jacobian. Next, a matrix of gradients $[B]$ is built and integrands of the form $[B]^T\,[D]\,[B]$, $[B]^T\,[D]\,\{A\}$ are calculated. After adding the contributions of the all elements we obtain the overall rigidity matrix.

In FEM implementation, the key program is that concerned with solving the system of algebraic equations. Naturally, it is desirable to obtain a solution as accurate as possible, with minimum machine time consumed, and without employing external computer storage. It is impossible to meet all these requirements simultaneously; therefore, we used the direct Gauss method of elimination, which provides an accuracy within the round-off error. For the purpose of saving the internal storage of the computer, the matrices were transformed to those of the band type. This is possible in the case of symmetrical matrices when a square $N \times N$ matrix is reduced to an $N \times m$ matrix, where m is the band halfwidth of the matrix. Using such an approach, we can solve a practically unlimited number of equations, provided a band width is restricted.

The data obtained upon solving a system of the initial equations, i.e., local values of the desired functions at the nodes of the elements, were processed using special subprograms that allowed integration along given directions and differentiation at the nodes as well as determination of the function norms at any step Δz_i, construction of isolines of the desired functions, and determination of the average characteristics (heat flux densities, a Nusselt number, finning efficiency, etc.).

Since the program does not provides for use of linear and square isoparametric elements, it is pertinent to note the following. With use of higher-order elements, there is no need to use the theory of consistent results of elements. In this case, the latter are functions of the coordinates and can be calculated at any arbitrary point. In the case of simplex elements, the values of the functions are constant in each element, which corresponds to a stepwise change on passing from one element to another. When higher-order elements are used, the distribution of the desired function is continuous. In this case, not only an amount of required initial data decreases but also the dimension of the resultant system of nodal equations.

Trial-Function Method. The numerical scheme was checked by the trial-function method, the essence of which lies in comparing an accurate solution obtained for some class of functions with a numerical solution for the present model.

We consider two functions that were used in checking the numerical scheme, i.e., linear and exponential. In the first case, the following trial function

$$\Phi = x + y + z\,, \tag{1.13}$$

is used, which, as is easily checked, represents a solution of the model equation

$$\frac{\partial\Phi}{\partial z} = -\frac{\partial^2\Phi}{\partial x^2} + \frac{\partial^2\Phi}{\partial^2 y} + 1 = 0\,. \tag{1.14}$$

In the second case, use is made of the rather often adopted exponential function

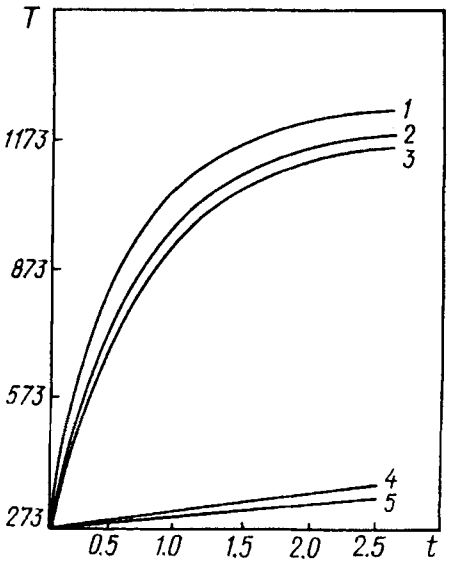

Fig. 4. Comparison of the temperatures calculated by the FEM-2.5; calculations of [6] - 1.3 and of the Central Fire Administration of the Republic of Belarus - 4 for heating of the 200 mm-thick concrete wall under standard fire conditions. Curve 4 is plotted for constant concrete properties, curves 2, 5 – for variable properties. T, K; t, h.

$$\Phi = \exp x + \exp y, \tag{1.15}$$

which is a solution of the differential equation

$$\frac{\partial \Phi}{\partial z} = -\frac{\partial^2 \Phi}{\partial x^2} - \frac{\partial^2 \Phi}{\partial^2 y} - \exp x + \exp y = 0. \tag{1.16}$$

In this case, values of the normal derivatives at the domain boundaries, respectively, exp x and exp y of the FEM solution coincide with the analytical solution to the fourth decimal place. A large set of trial functions can be presented which provide good agreement when checking the numerical scheme.

Sometimes the trial-function method acquires a physical meaning when a definite comparison with a physical calculation is made, for instance, in the problem of temperature field determination in a uniform rod. Such a problem is easily solved analytically and then compared with the numerical FEM-solution.

An analytical solution can be obtained from the heat conduction equation using, e.g., the method of separation of variables

$$T = Ax + By + C \tag{1.17}$$

and determining the constants A, B, and C from the boundary conditions. In final form, it can be written as follows:

$$T = T_1 - \frac{\Delta T}{\Delta x} x, \tag{1.18}$$

where T_1 is the temperature at the left-hand boundary of the rod ΔT is the temperature difference in the rod; Δx is the rod length. The values obtained using the FEM model fully coincide with the analytical solution.

A similar test was carried out to check the second-kind boundary conditions at the end of the rod. For this, the specific heat flux was prescribed at the free boundary of the rod, which was chosen, for convenience and easy interpretation, so that the temperature drop differential neighbouring nodes was constant, e.g., 10 K. In this case, the temperature distribution along the rod was linear and the FEM-solution coincided with the analytical one with accuracy to the fourth decimal place.

Finally, the nonstationary problems of heating of a brick wall [7] under third-kind boundary conditions (convective heat transfer over heated and cooled surfaces) and of a concrete flat wall under standard fire conditions [6] were calculated. In both cases, the discrepancies in the calculations did not exceed 1.5–2.0%. Results of a comparison of the FEM solution with the data of [6] with respect to the heating time of a concrete wall under standard fire conditions are represented in Fig. 4.

2. NUMERICAL STUDIES AND DISCUSSION OF RESULTS

A calculation model of a wall section is shown in Fig. 2. For the purpose of reducing the volume of calculations, without worsening the quality of the information obtained, the integration domain is restricted by the lines of symmetry (the left- and right-hand boundaries of the model in the figure). The fragment width was equal to a half of the nominal length of the block, i.e., 200 mm, while the thickness was the designed thickness of the wall. The fin thickness was assumed equal to its mean value with respect to the block height. The air temperature for fire spreading from the side of the heated surface [6] was determined as a function of the time of continuous fire attack τ:

$$T_{air} = 345 \log (0.135\tau + 1) + T_{in} . \tag{2.1}$$

The air temperature from the side of the unheated surface was assumed to be constant and equal to 20°C. Before a fire, the initial temperature T_{in} of the construction was 20°C.

In modeling heat transfer between a heated gas and a wall, the process of thermal radiation plays an important role. Usually in heat engineering designs it is determined, by analogy with convective heat transfer, using the radiative heat transfer coefficient α_r. The latter is defined as the quotient of the heat flux q and the temperature head.

The coefficient of heat transfer α to the wall surface heated under fire conditions was determined from the relation [6]:

$$\alpha = 29 + (3.9 - 0.0023t_0) \frac{(t_{air}/100)^4 - (t_0/100)^4}{t_{air} - t_0} , \tag{2.2}$$

where t_0 is the temperature of the heated surface, K; t_{air} is the air temperature during a fire.

The specificity of this problem lies in the high temperature heads as viewed from the heated wall. With such a formulation it was necessary to solve initial equation (1.1) with changing thermophysical properties, dependent on temperature, and variable boundary conditions, which change with time according to the law determined by Eqs. (2.1) and (2.2).

The thermophysical properties of wall materials were calculated using polynomial approximations and relations given in [6]. For air, the properties were determined by interpolation using tabular values in the investigated temperature range. It should be noted that use of the variable material properties and boundary conditions, dependent on time, makes this problem substantially nonlinear and requires sufficiently small time steps in solving Eq. (2.1) numerically.

Area Quantization. Temperature Profiles in the Wall. The finite-element model of the calculated region consisted of 144 elements and 483 nodes at which temperature values were calculated. The possibility of automatic generation of the finite-element network allowed the choice of an optimal, with respect to the required accuracy and processing time, number of elements and network thicknening in the regions of expected maximum temperature gradients. For the sake of convenience and pictorial representation, the digital data on temperature calculation were represented in the form of temperature isolines (isotherms) calculated and built for different moments of time from the beginning of fire spreading. Each of the calculation versions included the isotherm T_{cont} = 500°C, as it was required in the technical task. In Fig. 5 it is marked by figure 10.

Figure 5a shows the temperature distribution 15 min later after the beginning of a fire. The isotherm T_{cont} = 500°C practically coincides with the heated surface. But 30 min after the beginning of the fire (Fig. 5b), the

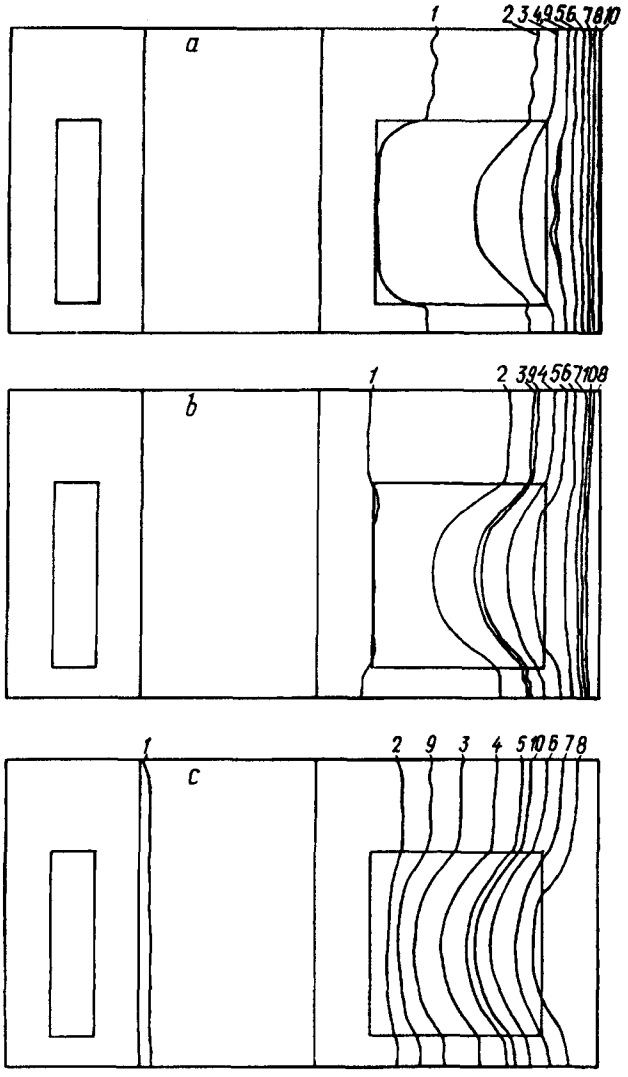

Fig. 5. Temperature distribution T, K (isotherms in the tested three-layer wall for standard-fire evolution: a) 15 min after the beginning of a fire; b) 30 min later; c) 135 min later. 1) 294 K; 2) 348; 3) 400; 4) 457; 5) 512; 6) 567; 7) 621; 8) 676; 9) 453; 10) 773 K.

isotherm runs at the distance of approximately 10–15 mm from the heated surface. The isotherm T_{cont} = 180°C was also constructed for each moment of time. The temperature distribution in Fig. 5b is indicative of the insignificant depth of block heating after the beginning of a fire and thus of, practically, full preservation of the load-bearing strength properties of the investigated concrete block for this period of time.

The further heating of the block for a period of up to 2.5 h from the moment of fire spreading was calculated with the time interval of 0.5 h (Fig. 5c). The maximum depth of concrete block heating to 500°C amounted to approximately 45% of its thickness (~75–80 mm) inside the air cavity and up to 32% of its thickness (~55–60 mm) with respect to the central and side walls.

CONCLUSIONS

1. A problem of calculation of the fire resistance of a three-layer wall consisting of concrete blocks fabricated according to the technology of the firm "BESSER" was formulated and solved.

The mathematical model of the heating process was based on an equation of unsteady heat conduction with nonlinear coefficients and boundary conditions dependent on time.

In the calculations, the applied problem-oriented software package NIKABT, developed by the author and adapted for the present problem, was used.

2. The reliability of the results obtained is confirmed by the adequacy of the physical and mathematical models of the investigated heat conduction process and by standard tests for such problems, which included:

a) checking of the numerical scheme by the trial-function method. Values of the trial functions obtained by the FEM method coincided with the exact analytical solutions to the fourth decimal place;

b) comparison with the results of solving the unsteady problem of brick-wall heating obtained by other authors [7]. The discrepancy between the FEM solution and the data of [7] did not exceed 1.5–2%;

c) comparison with the results of solution of the unsteady problem of flat concrete wall heating in the case of standard fire evolution. The discrepancy between the FEM solution and the data of [6] did not exceed 1.5%.

Results of the comparisons confirm the validity of problem formulation and the reliability of the data obtained in calculations.

3. Calculations were made for fire evolution of up to 2.5 hours of real time. An analysis of the results showed that 0.5 h after fire spreading the isotherm $T = 500^{\circ}C$ was at a distance of 10–15 mm from the heated surface, which was less than a half of the thickness of the load-bearing fin of the concrete block as viewed from the fire ($\delta_{fin} = 37$ mm).

The maximum depth of heating to 500°C, which was reached 2.5 h after the beginning of the fire, was from 55 to 80 mm, as viewed from the fire, which corresponded to 32–45% of the mean block thickness.

REFERENCES

1. A. A. Mikhalevich, V. I. Nikolaev, and V. K. Fedosova, Inzh.-Fiz. Zh., 57, No. 2, 246-253 (1989).
2. A. A. Mikhalevich, V. I. Nikolaev, and V. K. Fedosova, Inzh.-Fiz. Zh., 59, No. 5, 747-757 (1990).
3. Stroit. Normy Belarusi 2.01.01-93 "Civel Housing Heat Engineering.
4. Stroit. Normy i Pravila 2.01.02-85* "Antifire Norms."
5. Stroit. Normy i Pravila 2.03.01-84* "Concrete and Reinforced Concrete Structures."
6. Recommendations for Determination of the Limits of Fire Resistance of Concrete and Reinforced Concrete Structures [in Russian], Minsk, Belarusian Research Institute for Reinforced Concrete (1986).
7. Recommendations for Designing Structures from Vibropressed Hollow Concrete Blocks [in Russian], Minsk, Belarusian Research Institute for Civil Engineering (1994).
8. A. I. Yakovlev, Calculation of Fire Resistance of Building Structures [in Russian], Moscow (1986).
9. E. R. Eckert and R. M. Dreick, Theory of Heat and Mass Transfer [Russian translation], Moscow (1961).